Micropatterned Liquid Crystalline Networks for Multipurpose Color Pixels

ACS APPLIED MATERIALS & INTERFACES

www.acsami.org
Research Article

Micropatterned Liquid Crystalline Networks for Multipurpose Color Pixels

Irina Zubritskaya,* Daniele Martella,* and Sara Nocentini*

Cite This: ACS Appl. Mater. Interfaces 2025, 17, 11100−11107
Read Online

ABSTRACT: Materials that can visually report changes in the surrounding environments are essential for future portable sensors that monitor temperature and detect hazardous chemicals. Ideal responsive materials for optical sensors are defined by a rapid response and readout, high selectivity, the ability to operate at room temperature, and simple microfabrication. However, because of the lack of viable materials and approaches, compact, passive, and multipurpose practical devices are still beyond reach. To address this challenge, we develop a methodology to fabricate colored and responsive micropixels printed by digital light projection lithography on gold substrates. These structures are made by polymeric Liquid Crystalline Networks (LCNs) whose birefringence and external stimuli responsiveness allow for micrometric devices with visual and fast response that we here apply to a few applications. First, we show how varying the projected geometrical shape can become an effective tool to engineer symmetric disclination lines in the liquid crystal order. Depending on the thickness of the micropixels, LCNs give rise to a birefringence color under polarized light or a structural color under white light due to thin-film interference. By exposing the micropatterns to temperature variation and solvents, we demonstrate a real-time optical temperature detection and differentiation between selected organic chemicals. The proposed materials and fabrication method could be scaled up and extended to roll-to-roll printing, enabling future real-life applications of liquid crystalline polymers in affordable microdevices and optical sensors with a net advantage with respect to traditional lithographic techniques in terms of fabrication speeds and costs.

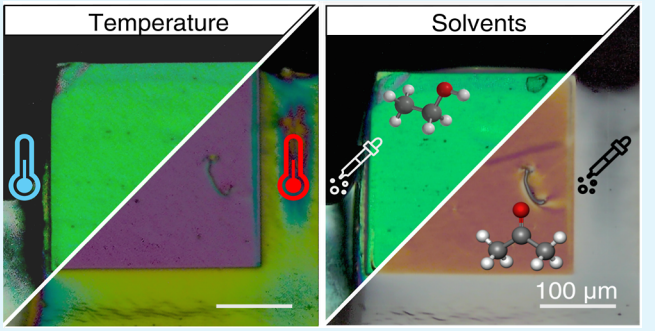

KEYWORDS: *liquid crystalline networks, multiresponsive materials, digital light projection lithography, microprinting, color pixels*

1. INTRODUCTION

Printing of responsive polymers on the micro- and nanoscale is becoming more and more important both in the industrial sector and scientific research, thanks to the progress in commercial instruments and material formulations.[1,2] Today, photopolymerization technologies allow for three-dimensional (3D) printing with nanometer precision by drawing on multiphoton and multistep absorption photochemistry.[3,4] These techniques proved well-suited for printing materials that respond to different stimuli (e.g., light and electric or magnetic fields) to break new ground for smart and miniaturized devices for advanced applications, for example, remotely controlled microrobots,[5−7] integrated photonics,[8,9] and smart microfluidic elements.[10] However, at this moment, writing speed remains the major limitation on using these techniques for serial manufacturing. When it comes to two-dimensional (2D) microprinting of polymers on a large scale, maskless digital light projection (DLP) lithography and roll-to-roll lithography currently present the best alternatives as fast and low-cost photolithographic techniques.[11−13] In contrast to traditional photolithography, maskless lithography requires no physical contact (e.g., no mask required for the exposure) and allows for a transfer of any digitally created pattern. This is carried out in one-step exposure using light projection, making DLP a faster, less expensive, and more accessible approach.

Among multi stimuli-responsive materials, nematic Liquid Crystalline Networks (LCNs) are polymeric systems particularly attractive as systems capable of programmable shape-morphing[14−16] and mechanical force generation that mimics natural muscles.[17,18] LCNs can be easily prepared by photopolymerization of a mixture of aligned reactive mesogens[16,19] to form an oriented polymeric network, where the liquid crystal (LC) units are attached to the polymer backbone.[20] A reversible shape-change, triggered by gradual disordering of the mesogens,[21] points out LCNs as future materials for compact sensors with continuous monitoring operation. The simplicity of preparation by photopolymerization allows translation of the

Received: November 27, 2024
Revised: December 23, 2024
Accepted: December 31, 2024
Published: February 4, 2025

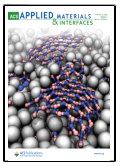

https://doi.org/10.1021/acsami.4c20865
ACS Appl. Mater. Interfaces 2025, 17, 11100−11107

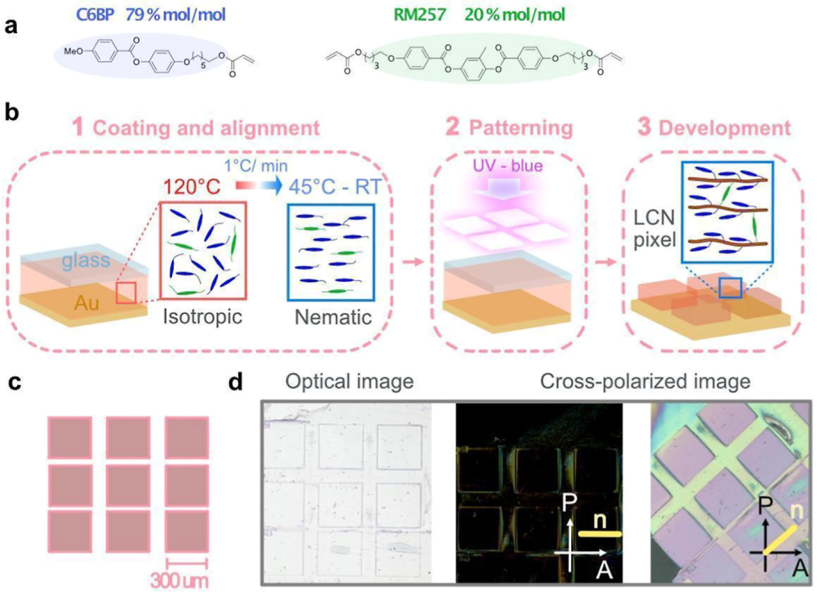

Figure 1. Materials and fabrication technique of LCN microscale pixels. (a) Mesogens used in the formulation. (b) Main steps for fabrication of microscale LCN pixels. (c) CAD layout of a square micropattern. (d) Optical and POM images of microscale pixels with LC director, *n*, oriented at 0 and 45° with respect to the polarizer and analyzer.

macroscale properties to the micrometer scale by adopting microfabrication approaches. Previously, microscale LCNs were obtained by soft lithography,[22,23] two-photon lithography,[24−27] capillary microfluidic process,[28] and DLP with or without masks.[29−31] However, in the latter case, LCNs were only printed by DLP as polydomains, which largely compromise their ability to change shape and the large variation in birefringence typical of homogeneously aligned samples.

In this work, we unveil the behavior of aligned microprinted LCNs. We first produce monodomain and spatially ordered microscale LCNs on metallic substrates by using a fast and scalable DLP lithography. In essence, we use a light projector to expose a digitized pattern onto a photopolymerizable LC monomer layer to define different micrometer-size pixels. The use of gold as substrate not only represents a technical development (where photolithography is generally carried out on glass or silicon wafer) but also enhances the interference colors of the patterns depending on the printing parameters. Following up our previous work on optical cavities made with LCNs and aluminum,[32] we now replace aluminum with gold and perform microprinting to further extend the application area of LCNs from tunable nanophotonic films to microdevices for sensing.

This technique serves many purposes, providing advantages on (i) stability and integration of the LCNs on different types of substrates, thanks to the polymeric nature of the materials; (ii) ease and low-cost fabrication suitable for large-scale production; and (iii) fast response enabled by the LCN formulation and device miniaturization. More in detail, we design diverse topological defects by playing on the printed geometric shape and produce LCN pixels that visually respond to temperature variation and exposure to selected organic solvents by shifting their polarization color. By exploiting the same fabrication technique on dye-doped LCN, we report a whole palette of interference subtractive coloration to white light illumination in lossy dielectric−metal micropixels. These results pave the way for new compact micro devices and microsensors for rapid detection of organic solvents that visually report changes in the environment using a simple and fast working mechanism.

2. EXPERIMENTAL SECTION

2.1. Materials. The monomer mixture contains mesogen C6BP (89% mol/mol), RM257 (10% mol/mol), and Irgacure 369 (1% mol/mol). C6BP (4-methoxybenzoic acid 4-(6-acryloyloxyhexyloxy)-phenylester) and RM257 (1,4-bis-[4-(3-acryloyloxypropyloxy)-benzoyloxy]-2-methylbenzene) are purchased from Synthon Chemicals; all other reagents are purchased from Merck.

2.2. LC Cell Preparation. Polymerization cells are assembled by dispensing the monomer mixture (at 120 °C) on a gold substrate and then by placing a top cover glass, which distributes the mixture by capillarity. The sample is cooled to 45 °C at a rate of 1 °C/min to the nematic phase and annealed for 30 min to reach the monodomain. The successful alignment is confirmed by polarized optical microscopy (POM) prior to patterning. The gold substrates are prepared by depositing 60 nm of gold at a rate 2 $Å s^{-1}$ onto silicon chips and annealed at 120 °C for 5 min on a hot plate. For homogeneous planar alignment, the glass is coated with a poly(vinyl alcohol) (PVA) solution (5% wt in water) that is spin coated at 3000 rpm, dried at 90 °C for 30 min, and rubbed using a velvet cloth. For homeotropic alignment, we used untreated and cleaned borosilicate glass.

2.3. DLP Patterning. Micropattern layouts are designed by CAD software (Klayout). The cells with the LC monomer are patterned using a DLP printer (3D Microlight) with a 435 nm lamp with a large depth of focus and 1920 × 1080 pixels' resolution. The microprinter employs a spatial light modulator with a beam splitter cube that produces linearly polarized light. We use a 10× objective giving a projected pixel size of 0.7 μm and ultraviolet (UV) light intensity 1019 mW/cm^2 that is focused on the bottom gold substrate. The pixel's height is controlled by varying the duration of light exposure in the interval 20−180 s and by adjusting the distance between the substrate and the objective lens. By playing with these two parameters, we can make in a single exposure step micropixels with a height from a few hundred nanometers to a few micrometers. For LCN micropixels used in temperature and chemical sensing, the maximum thickness (2.2 μm) was reached using the exposure time 60 s. For fundamental subtractive colors, we use 125 s to obtain blue, 145 s to obtain yellow, and 105 s for magenta pixels. For the array of ultrathin LCN pixels in Figure 5d, the exposure dose is varied by adjusting the distance between the substrate and the objective lens at

https://doi.org/10.1021/acsami.4c20865
ACS Appl. Mater. Interfaces 2025, 17, 11100−11107

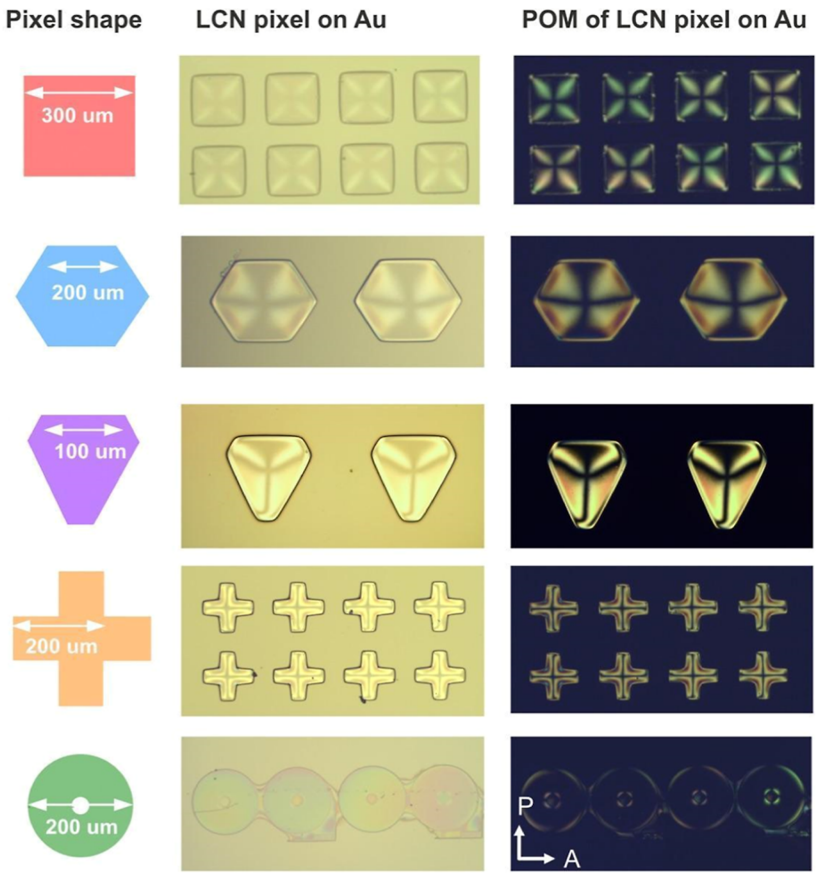

Figure 2. Formation of multidomain and topological defects via micropixel shape design. Microprinting of 2D pixels with different shapes (left panel) impresses complex LC alignment (central and right panel). One-fold rotational symmetry and donut geometry preserves initially homeotropic alignment while multifaceted geometry introduces nontrivial disclination lines and point defects.

fixed exposure time 90 s. After patterning, the cells are developed in isopropanol at 70 °C for 1−2 h.

2.4. Non Patterned LCN Film. A LC cell was assembled using the same monomer mixture and methodology described above. The monomeric mixture (same used for the micropixels) has been placed in between a glass substrate sputtered with 60 nm of gold and a unidirectionally rubbed PVA layer. After the infiltration, the cell has been photopolymerized by UV irradiation (LED lamp Thorlabs M385L2-C4, 385 nm, 110 mW) at room temperature for 10 min and then, the glass has been removed manually to obtain the final sample on gold.

2.5. Material Characterization. POM is performed with an Zeiss Axio Observer A1 microscope in the cross-polarized mode equipped with a Linkam PE120 hot stage and an Axio camera. Height topographies of the micropixels are measured by a Sensofar S-Neox optical profilometer.

3. RESULTS AND DISCUSSION

3.1. Micropatterning and Spatial Alignment Control. The LCN microscale patterns on gold-coated substrates are prepared by free-radical photopolymerization starting from a formulation of acrylate-based reactive mesogens. The structure and composition of the monomer mixture are reported in Figure 1a.

The monomers are melted in the isotropic phase and infiltrated by capillary action in a thin cell (consisting of a bottom gold substrate and a top cover glass) and then cooled to obtain a monodomain alignment in the nematic phase (Figure 1b). After the LC alignment is confirmed by POM, DLP lithography is used to expose the microscale light patterns onto the mixture (Figure 1c) at room temperature. In this process, light from a broadband UV source is projected using a spatial light modulator, which creates a cross-linked polymer network in the exposed regions. As a last step, a development bath is used to remove the unpolymerized mixture, thus leaving LCN micropixels with the desired CAD-shape on the metal substrate (Figure 1d, left panel).

Following this protocol, we created microstructures on gold-coated substrates starting from both planar homogeneous and homeotropic aligned monomer mixtures using similar conditions. Within this technique, maintaining the initial alignment of the mixture after polymerization is not trivial and requires a specific precaution before the patterning. Indeed, to guarantee the retention of homogeneous planar alignment, a prepolymerization step is carried out to stabilize the alignment and then, the final microstructures are defined by exposing the micropattern (Figure 1d). The prepolymerization is implemented by exposing the entire cell to a very low radiation dose (5−10% of the minimal dose needed to fully polymerize the monomer). The alignment is verified by POM, which shows a maximum in reflectance at 45° and full extinction at 0°-orientation of LC director n with respect to polarizer and analyzer (Figure 1d) as expected for a homogeneous planar aligned LC. The light green background beneath the purple microsquares in the cross-polarized image (Figure 1d) reveals a background LCN layer that is formed in the prepolymerization step, with different birefringence colors corresponding to different thicknesses.

On the other hand, if the prepolymerization step is skipped, the unconstrained LC alignment evolves during the exposure

https://doi.org/10.1021/acsami.4c20865
ACS Appl. Mater. Interfaces 2025, 17, 11100−11107

step, giving rise to highly symmetric topological defects within a printed micropixel. The DLP-induced alignment evolution and topological defect formation are observed in thin polymerization cells with thicknesses of a few micrometers. Each geometrical shape of the projected pixel impresses its unique features on the orientation of the LC director, which is fully repeatable. Figure 2 shows how, starting from an initially homeotropic mixture, a variety of topological point defects and disclination lines can be obtained, depending only on the projected geometrical shape. In case of a square shape, a point defect emerges in the center of the structure, whereas for a cross shape, two disclination lines intersect in the center. We study the influence of the shape's boundaries on the resulting alignment patterns by printing multifaceted shapes with different lengths, facet orientation, and symmetry (e.g., a shield, a pentagon, and a donut). In general, the LC director profile is the result of the balance of the surface anchoring and the bulk elastic energies to minimize the total free energy of the system. However, along the polymerization process of the thin LC cells, the orientational order of the initial homeotropic alignment is strongly affected by the topological constraints imposed by the polymerized shapes and the diffusion properties of the LC mesogens.[33] The photopolymerization through a photomask or a DLP projection causes molecular diffusion at the boundary between the exposed and unexposed areas determining a local shear stress.[34] By changing the printed shapes, the LC anchoring at the edges of the structure is perturbed, and the monomer diffusion into the polymerized region determines the defect formation. We deduce from cross-polarized images in Figure 2 that monomers that flow across the boundaries create a disclination line where they meet together. This effect can be attributed to the diffusion of low-weight LC monomers from monomer-rich regions (unexposed areas) to regions with monomer depletion (partially polymerized areas).[35,36]

Interestingly, no deviation from the initial homeotropic state is observed when the shape geometry has a one-fold rotational symmetry with respect to the homeotropic LC director and a donut shape. This shape-dependent behavior can be attributed to an isotropic diffusion and uniform radial alignment at the shape edges. Similar effects can be observed also starting from LC cells with homogeneous planar alignment, thus confirming empirically that the forces that drive the alignment distortion are stronger than the anchoring imposed by the surfaces of the glass cell also for different heights of the micropixels (Figure S1).

We thus present a new way to create complex LC multidomain patterns with topological defects by shape-design that would otherwise only be possible by a spatially modulated photoalignment process.[37−39] This methodology can also be extended to the realization of sensors or photonic applications as previously reported for topological defects of LCs.[40,41]

In the following paragraphs, we showcase the versatility of DLP fabrication of responsive birefringent materials by highlighting different potential applications of microprinted LCN.

3.2. Polarization Color LCN Micropixels and Their Multiresponsive Behavior. Birefringent materials observed at POM give rise to polarization color that depends on the sample thickness and the optical anisotropy. Only the polarized light (wavelength) for which the accumulated phase difference [$\delta = 2\pi(\Delta n \times t)/\lambda$, where Δn is the birefringence, t is the sample thickness, and λ is the wavelength] in between the fast and slow axis is $\pi/2$ pass through the analyzer giving rise to the polarization color. By knowing the birefringence and the sample thickness, the Michel-Levy chart can then be used to reconstruct all the polarization colors for birefringent samples. Exploiting this property of LCN, we first study the polarization color dependence to external stimuli for a multipurpose microsensor. This mechanism allows for the sensing of any stimulus that can produce a notable change in either of these properties by monitoring the polarization color. Temperature-sensitive polarization color in transmission was previously reported in thick LCN microstructures obtained by two-photon 3D printing.[42] In our work, we use a simple microprinting technique and implement the monitoring in the reflection configuration (on the gold substrate) that intensifies the color by phase-shifting light by π radians. To associate the observed coloration with the thickness, we characterize the height of the micropixel array with homogeneous planar alignment reported also in Figure 1d with an optical profilometer (Figure S2). The pixels have a total height of around 2.2 μm, including a background layer underneath with a height of 1.8 μm. This geometry results in pink LCN micropixels on a light green background (during POM observation in reflection). To get a better insight into these data, we analyze the resulting polarization colors by comparing it with the Michel-Lévy chart,[43] taking into account that light travels through the film twice in reflection. Knowing the sample thickness and the resulting polarization color, we retrieve the LCN sample birefringence that is around $\Delta n = 0.35$ (Figure S2), a value that is consistent with other recently reported measurements.[44]

Here, we show experimentally how micropatterned LCN with retained homogeneous LC order respond to multiple stimuli. In Figure 3, we analyze how the reflected and polarization colors

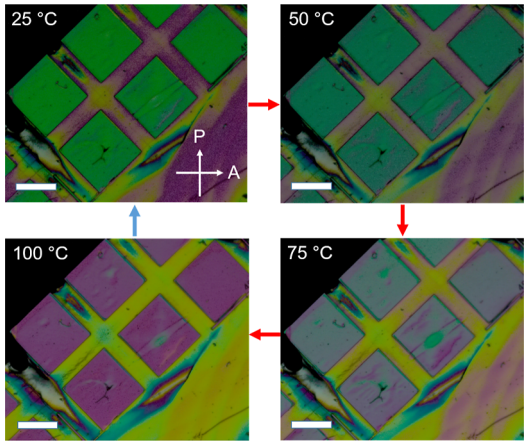

Figure 3. Thermoresponsive behavior of LCN micropixels. POM images during a heating cycle at 25, 50, 75, and 100 °C. The color is reversible by cooling (blue arrow). Images are taken with the nematic director oriented at 45° with respect to the polarizers. Scale bar: 200 μm.

respond to temperature variation. During a heating cycle, we observe a gradual color variation of the squares from green to magenta and of the background from magenta to yellow. The color variation is fully reversible upon cooling to room temperature. The polarization color change can be attributed to either the height or birefringence variation, or likely both with one being more dominant. To get a better insight into how either of them contribute to color change, we analyze them in detail. If we suppose that the birefringence is constant along the heating cycle, the color change should be attributed to a height

https://doi.org/10.1021/acsami.4c20865
ACS Appl. Mater. Interfaces 2025, 17, 11100−11107

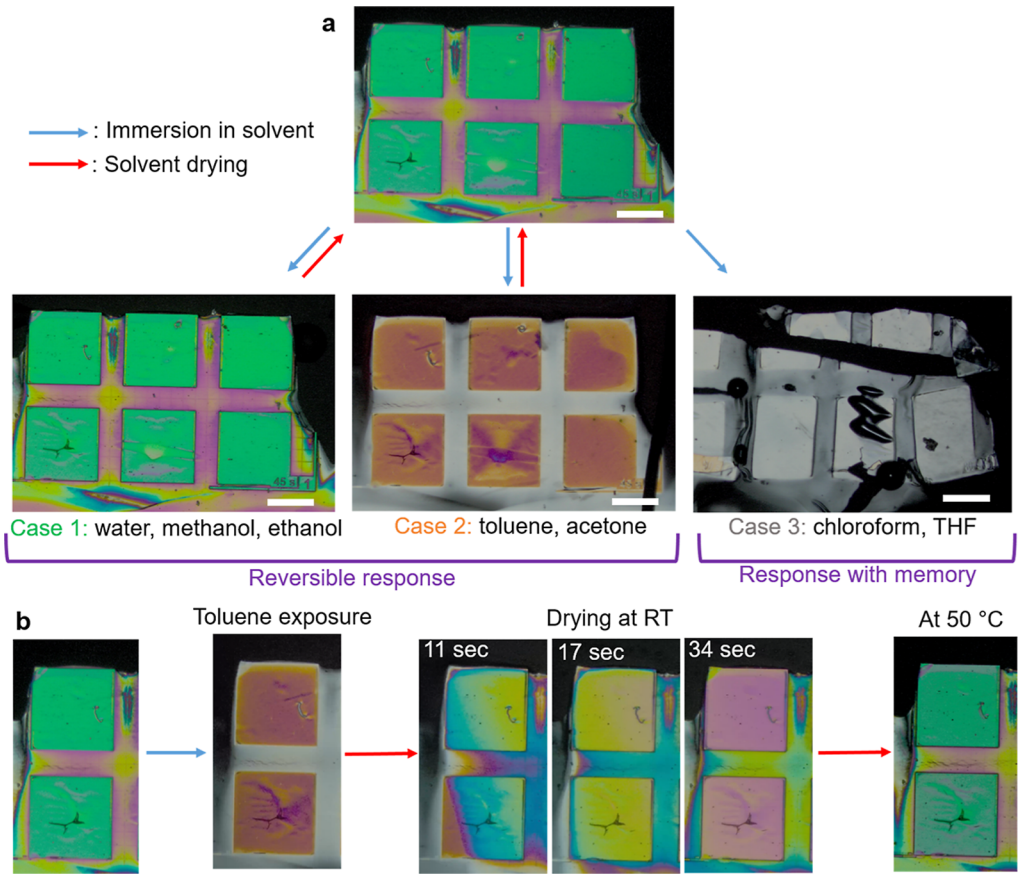

Figure 4. Chemo-responsive behavior of LCN micropixels. (a) POM images of LCN micropixels in air (top line) and after immersion in different solvents (bottom lines). Depending on the solvents, the LCNs acquire a different color and shape. (b) Insight into chemo-responsive behavior of a LCN pattern. After immersion in toluene, the micropixels change color from green to orange-brown in 5 s. After solvent evaporation at room temperature (RT), the pattern acquired different colors to recover the initial (green) state by drying at 50 °C.

expansion of around 28% (500 nm) with a relative orthogonal contraction of at least 51 μm (in the 300 μm-squares, see Figure S3). As shown in Figure 3, the polarization color change is not accompanied by a measurable shape change of the thin microstructures due to the strong constraint impressed by the substrate. It can therefore be mainly attributed to the partial internal network disordering with a net loss in birefringence from 0.35 to 0.29, which is retrieved from the Michel-Levy chart (Figure S3). To prove the consistency in results, we analyze a similar pattern with slightly different heights using the Michel-Lévy chart and show how it responds to the temperature change in Figure S4.

The LCN's molecular structure enables color micropixels that respond not only to temperature but also to chemical stimuli. Indeed, chemical adsorption processes can modify the shape of LCN[45,46] or their birefringence due to selective swelling processes that is an intrinsic feature of this aligned material. This makes LCNs, especially in their microprinted version, a suitable platform for sensing of organic compounds (including solvent or volatile organic compounds—VOCs) that could be present as contaminants in the environment. To date, only few studies demonstrated how macroscale acrylate-based LCNs can be employed as chemo-responsive actuators, whose dimension can change because of anisotropic swelling in selected solvents.[45,46] These studies provide a fundamental insight into chemo-responsive behavior of macroscale LCNs, whereas the capabilities of microprinted LCN in chemical sensing remain completely unexplored. To fill this gap, we investigate how microprinted LCNs respond to solvents with different degrees of polarity and chemical structure. Figure 4 shows how initially green micropixels change color when exposed to a specific chemical stimulus. Three cases of different color variations are identified in Figure 4a. In case 1, the immersion in polar solvents, such as water, methanol, or ethanol, does not cause any variation in the color of pixels. This behavior suggests the absence of swelling of our LCN in these solvents. The unchanged green color in these wet environments indicates that the pixels do not exhibit any shape-deformation or birefringence variation.

On the other hand, for immersion in other organic solvents, the response depends on the type of solvent. For toluene and acetone (case 2), the micropixel's color shifts from green to orange-brown as fast as in 5 s and vice versa after the solvent evaporation with a temporal recovery that is ruled by the evaporation process. Such color change due to birefringence variation being an intrinsic materials property is also observed for large-film areas (see Figure S5). In this example, the polymeric film has been prepared by the same LC cell filled with the monomer mixture and polymerized by the exposure with an UV light. Even if different polymerization approaches could lead to small variations of the cross-linking degree, the qualitative comparison in between the two samples demonstrates clear advantages offered by the micropatterning in the chemo-response. At first, micropixels are characterized with a height and thus color uniformity that makes them suitable for color change detection while large film thickness uniformity is more challenging. Moreover, in small patterned pixels, solvent

https://doi.org/10.1021/acsami.4c20865
ACS Appl. Mater. Interfaces 2025, 17, 11100−11107

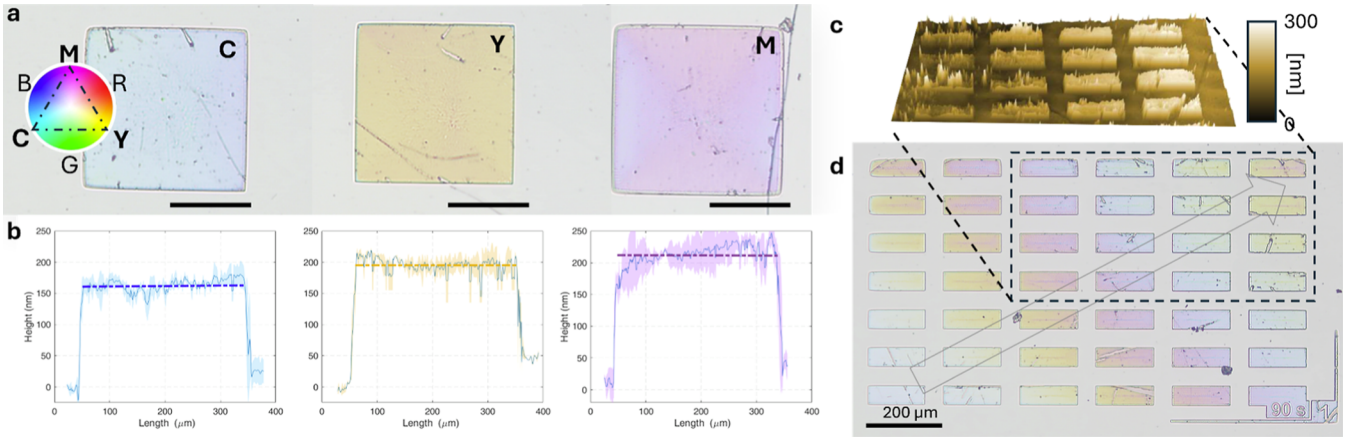

Figure 5. Structural colors by ultrathin LCN micropixels. (a) Optical image of LCN pixels showing fundamental subtractive colors: cyan, yellow, and magenta that correspond to different heights (b). Optical profilometer measurements and their standard deviation (shaded area) obtained for four consecutive measurements of the LCN height for each color reported in Figure 5a. The dashed lines refer to the average height that for the different colors is 165, 195, and 215 nm, respectively. (c) 3D reconstruction of the topography of the LCN micropixels that shows how different colors correspond to different thicknesses of the lossy dielectric cavities. (d) Optical image of LCN micropixels with different heights, the arrow indicated the increase in height. By tuning the structure height, the whole palette of subtractive colors can be obtained.

swelling produces larger color variation in shorter time with a typical evolution that lasts in a few seconds in micropixels instead of tens of seconds typical for planar film color change. We can attribute this difference to the reduced dimensions of the pixels, the larger contact surface with the solvent, and the lower anchoring to the gold substrate.

When we expose micropixels to other organic solvents, such as tetrahydrofuran (THF) or chloroform, we observe simultaneously a color change (from green to colorless gray) and a notable shape-change of the pixels leading to permanent delamination (case 3). By comparing the pixel's dimensions before and after THF/chloroform exposure, we find that the pixel's expanded by 17% perpendicularly to the LC director and contracted along the LC director. Looking at a single square pixel, we observe how the structure suffers large swelling and pronounced irreversible anisotropic deformation (from aspect ratio 1 to around 2) compared to other solvents. After drying, we observe a partial color recovery, with no restoration of the original shape.

For the reversible process (case 2), we study the restoration of the polarization color during solvent drying in time. In Figure 4b, we show how the color changes at room temperature: the orange-brown pixels turn blue, then green-yellow, and then purple after 35 s. Heating to 50 °C can speed up the recovery of the initial green color and evaporate the residual solvent adsorbed by the polymer. In this example, there is a minor shape variation of the micropixels (2.5% contraction along the director in the presence of the solvent with respect to original shape), which cannot explain the observed color change if we assume an isotropic in-plane deformation (i.e., an expansion of the height of 50 nm that would correspond to coloration that are not experimentally observed). In accordance with the Michel-Levy chart, this optical effect color change can be mainly attributed to a birefringence variation from Δn = 0.35 to Δn = 0.11 (see Figure S6). To highlight the fast dynamics of the LCN micropixel response to toluene exposure, we record a video with real time speed in Movie S1.

With this simple visual sensor, we thus demonstrate how to discriminate between different organic solvents that can present a danger for human health or the environment such as toluene or chloroform by observing either a reversible polarization color variation or a permanent shape modification. In the latter case, the shape can be utilized as a memory to track back the chloroform presence.

3.3. Generation of Structural Colors by Ultrathin LCN Micropixels. Finally, we showcase a capability of DLP microprinting of LCN on gold-coated substrates to generate a gamut of interference colors in Figure 5. DLP is employed to pattern LCN micropixels with a set of subwavelength thicknesses and corresponding colors, known as interference, or structural colors. Structural colors can be observed in subwavelength thin-films, or in multilayer nanostructures, wherein the structural coloration can be enhanced by Fabry–Perot cavities with symmetric or asymmetric geometries.[47]

Herein, we demonstrate structural colors that are due to the thin-film interference in asymmetric lossy dielectric–metal structures that allow an easier fabrication process and no angular-dependent response with respect to traditional Fabry–Perot-type cavities.[48] Figure 5 shows how fundamental subtractive colors—cyan, yellow, and magenta—can be produced by ultrathin LCN pixels (thicknesses below 200 nm) by adding a small amount of dye (1 wt %, absorption peak at 520 nm) to the monomer mixtures.[24] The final pixels are composed of absorbing LCN and gold, acting as a mirror. The dispersion of gold's and dye's absorption in the LCN together contribute to the final structural coloration.[49]

By micropatterning thin layers of absorbing LCN with different heights, we obtain the three fundamental subtractive colors reported in the CIE chromaticity diagram (inset in Figure 5a). The difference in LCN height as small as 50 nm (LCN thickness range is 150–200 nm) enables the generation of the cyan, magenta, and yellow colors (Figure 5a). By progressively increasing the height of the micropixels (Figure 5b,c), we obtain the whole palette of subtractive colors (Figure 5d). In contrast to polarization colors, structural colors do not need a polarizer and can be seen with a naked-eye, which can find applications in pigment-free sustainable coatings and prints for visual appearance and color.

4. CONCLUSIONS

This study demonstrates the versatility of DLP lithography in engineering of multistimuli responsive microstructures for

https://doi.org/10.1021/acsami.4c20865
ACS Appl. Mater. Interfaces 2025, 17, 11100–11107

applications in chemical sensing, structural color printing, and topological defect design. We explore the capabilities and advantages of DLP for patterning of LCN as maskless, affordable, fast, and highly flexible fabrication technique. Our method can be adapted to many applications because it allows us to range the micropixel height from several micrometers down to hundreds of nanometers and below. We show for the first time how varying the shape geometry of the projected light pattern can be used to create highly symmetric topological defects in the LC alignment without the need for complex photoaligning techniques. By exploiting a micrometer-thick micropixel array, we produce polarized color pixels that work as visual sensors in response to temperature and exposure to selected organic solvents. These microsensors are able to discriminate between solvents by reporting a nonmodified, modified-reversible or irreversible polarization color or shape variation. We envision that the nonreversible shape transformation can be further exploited in smart sensors with memory of hazardous events and ability to capture and store an analyte. This mechanism could be particularly useful in monitoring major spills and leaks of hazardous and toxic agents after proper material optimization. Moreover, the chemo-responsive behavior of these micropixels can be further adapted for detection of specific compounds by appropriately tuning their selective adsorption. Our technology could be applied both for vapor and liquid sensing, advancing the state-of-the-art of other LC sensors.[50,51] For examples, polymer-stabilized LCs at a low cross-linking degree have been used to monitor temperature variation and toluene concentration, however limited in their integration capability as well as response time (from tens of minutes to hours).[50,51]

Lastly, we apply principles of nanophotonics to design ultrathin LCN micropixels that display fundamental subtractive colors for applications in photonic color prints. By shrinking down the thickness of the LCN micropixels, we demonstrate a gamut of structural colors that can be seen with the naked eye under white light illumination. All of these examples demonstrate how our technology can be adopted in a variety of photonic applications, from LC alignment engineering to tunable color coatings and prints, enabling the next-generation of optical devices and sensors.

■ ASSOCIATED CONTENT

Supporting Information

The Supporting Information is available free of charge at https://pubs.acs.org/doi/10.1021/acsami.4c20865.

Profilometer analysis and Michel-Levy chart interpretation for the observed polarized color pixels and examples of thermo- and chemo-responsive color change (PDF)

Fast color-change of a LCN micropixel array in contact with toluene (AVI)

■ AUTHOR INFORMATION

Corresponding Authors

Irina Zubritskaya − *Nanofabrication Laboratory (NFL), Department of Microtechnology and Nanoscience -MC2, Chalmers University of Technology, SE-412 96 Göteborg, Sweden*; Email: irinaz@chalmers.se

Daniele Martella − *European Laboratory for Non-Linear Spectroscopy (LENS), 50019 Sesto Fiorentino, Italy; Department of Chemistry, University of Florence, 50019 Sesto Fiorentino, Italy*; orcid.org/0000-0002-8845-0908; Email: daniele.martella@unifi.it

Sara Nocentini − *European Laboratory for Non-Linear Spectroscopy (LENS), 50019 Sesto Fiorentino, Italy; Istituto Nazionale di Ricerca Metrologica (INRiM), 10135 Torino, Italy*; orcid.org/0000-0003-2392-9077; Email: s.nocentini@inrim.it

Complete contact information is available at: https://pubs.acs.org/10.1021/acsami.4c20865

Author Contributions

I.Z. developed the methods and fabricated the micropixels. I.Z., M.D., and S.N. performed the characterization experiments and wrote the manuscript.

Funding

I.Z. acknowledges the Knut and Alice Wallenberg Foundation (Award 2017.0466) and the Carl Trygger Foundation (Award CTS 20:495) for funding. This publication has been funded by the Italian Ministry of University and Research (MUR) in the framework of the continuing-nature project "NEXT- GENERATION METROLOGY", under the allocation of the Ordinary Fund for research institutions (FOE) 2023 (Ministry Decree n. 789/2023).

Notes

The authors declare no competing financial interest.

■ ACKNOWLEDGMENTS

Part of this work was performed using the Swedish Research Infrastructure for micro- and nanofabrication Myfab and MC2 nanofabrication facility at Chalmers. D.M. and S.N. acknowledge CNR-FOE-LENS-2023.

■ REFERENCES

(1) Spiegel, C. A.; Hippler, M.; Münchinger, A.; Bastmeyer, M.; Barner-Kowollik, C.; Wegener, M.; Blasco, E. 4D printing at the microscale. *Adv. Funct. Mater.* **2020**, *30*, 1907615.

(2) Zhou, L. Y.; Fu, J.; He, Y. A review of 3D printing technologies for soft polymer materials. *Adv. Funct. Mater.* **2020**, *30*, 2000187.

(3) O'Halloran, S.; Pandit, A.; Heise, A.; Kellett, A. Two-photon polymerization: fundamentals, materials, and chemical modification strategies. *Adv. Sci.* **2023**, *10*, 2204072.

(4) Hahn, V.; Messer, T.; Bojanowski, N. M.; Curticean, E. R.; Wacker, I.; Schröder, R. R.; Blasco, E.; Wegener, M. Two-step absorption instead of two-photon absorption in 3D nanoprinting. *Nat. Photonics* **2021**, *15*, 932−938.

(5) Zeng, H.; Wasylczyk, P.; Wiersma, D. S.; Priimagi, A. Light robots: bridging the gap between microrobotics and photomechanics in soft materials. *Adv. Mater.* **2018**, *30*, 1703554.

(6) Dabbagh, S. R.; Sarabi, M. R.; Birtek, M. T.; Seyfi, S.; Sitti, M.; Tasoglu, S. 3D-printed microrobots from design to translation. *Nat. Commun.* **2022**, *13*, 5875.

(7) Martella, D.; Nocentini, S.; Nuzhdin, D.; Parmeggiani, C.; Wiersma, D. S. Photonic microhand with autonomous action. *Adv. Mater.* **2017**, *29*, 1704047.

(8) Zanotto, S.; Sgrignuoli, F.; Nocentini, S.; Martella, D.; Parmeggiani, C.; Wiersma, D. S. Multichannel remote polarization control enabled by nanostructured liquid crystalline networks. *Appl. Phys. Lett.* **2019**, *114*, 201103.

(9) Nocentini, S.; Riboli, F.; Burresi, M.; Martella, D.; Parmeggiani, C.; Wiersma, D. S. Three-dimensional photonic circuits in rigid and soft polymers tunable by light. *ACS Photonics* **2018**, *5*, 3222−3230.

(10) Ter Schiphorst, J.; Coleman, S.; Stumpel, J. E.; Ben Azouz, A.; Diamond, D.; Schenning, A. P. Molecular design of light-responsive hydrogels, for in situ generation of fast and reversible valves for microfluidic applications. *Chem. Mater.* **2015**, *27*, 5925−5931.

(11) Boyer, C.; Blasco, E.; Ke, C. Advanced 3D/4D Printing for Functional Materials Innovation. *Adv. Mater. Technol.* **2023**, *8*, 2301869.
(12) De Bellis, I.; Nocentini, S.; Delli Santi, M. G.; Martella, D.; Parmeggiani, C.; Zanotto, S.; Wiersma, D. S. Two-Photon Laser Writing of Soft Responsive Polymers via Temperature-Controlled Polymerization. *Laser Photonics Rev.* **2021**, *15*, 2100090.
(13) del Barrio, J.; Sánchez-Somolinos, C. Light to shape the future: from photolithography to 4D printing. *Adv. Opt. Mater.* **2019**, *7*, 1900598.
(14) White, T. J.; Broer, D. J. Programmable and adaptive mechanics with liquid crystal polymer networks and elastomers. *Nat. Mater.* **2015**, *14*, 1087−1098.
(15) Kularatne, R. S.; Kim, H.; Boothby, J. M.; Ware, T. H. Liquid crystal elastomer actuators: Synthesis, alignment, and applications. *J. Polym. Sci., Part B: Polym. Phys.* **2017**, *55*, 395−411.
(16) Liu, D.; Broer, D. J. Liquid crystal polymer networks: preparation, properties, and applications of films with patterned molecular alignment. *Langmuir* **2014**, *30*, 13499−13509.
(17) Thomsen, D. L.; Keller, P.; Naciri, J.; Pink, R.; Jeon, H.; Shenoy, D.; Ratna, B. R. Liquid crystal elastomers with mechanical properties of a muscle. *Macromolecules* **2001**, *34*, 5868−5875.
(18) Donato, S.; Martella, D.; Salzano de Luna, M.; Arecchi, G.; Querceto, S.; Ferrantini, C.; Sacconi, L.; Brient, P.; Chatard, C.; Graillot, A.; et al. The Role of Crosslinker Molecular Structure on Mechanical and Light-Actuation Properties in Liquid Crystalline Networks. *Macromol. Rapid Commun.* **2023**, *44*, 2200958.
(19) Martella, D.; et al. Cell instructive Liquid Crystalline Networks for myotube formation. *iScience* **2021**, *24*, 103077.
(20) Ohm, C.; Brehmer, M.; Zentel, R. Liquid crystalline elastomers as actuators and sensors. *Adv. Mater.* **2010**, *22*, 3366.
(21) Herbert, K. M.; Fowler, H. E.; McCracken, J. M.; Schlafmann, K. R.; Koch, J. A.; White, T. J. Synthesis and alignment of liquid crystalline elastomers. *Nat. Rev. Mater.* **2022**, *7*, 23−38.
(22) Buguin, A.; Li, M. H.; Silberzan, P.; Ladoux, B.; Keller, P. Micro-actuators: When artificial muscles made of nematic liquid crystal elastomers meet soft lithography. *J. Am. Chem. Soc.* **2006**, *128*, 1088−1089.
(23) Yang, H.; Buguin, A.; Taulemesse, J. M.; Kaneko, K.; Méry, S.; Bergeret, A.; Keller, P. Micron-sized main-chain liquid crystalline elastomer actuators with ultralarge amplitude contractions. *J. Am. Chem. Soc.* **2009**, *131*, 15000−15004.
(24) Zeng, H.; Martella, D.; Wasylczyk, P.; Cerretti, G.; Lavocat, J. C. G.; Ho, C. H.; Parmeggiani, C.; Wiersma, D. S. High-resolution 3D direct laser writing for liquid-crystalline elastomer microstructures. *Adv. Mater.* **2014**, *26*, 2319−2322.
(25) Donato, S.; Nocentini, S.; Martella, D.; Kolagatla, S.; Wiersma, D. S.; Parmeggiani, C.; Delaney, C.; Florea, L. Liquid Crystalline Network Microstructures for Stimuli Responsive Labels with Multi-Level Encryption. *Small* **2023**, *20*, 2306802.
(26) De Bellis, I.; Martella, D.; Parmeggiani, C.; Wiersma, D. S.; Nocentini, S. Temperature Tunable 4D Polymeric Photonic Crystals. *Adv. Funct. Mater.* **2023**, *33*, 2213162.
(27) del Pozo, M.; Delaney, C.; Pilz da Cunha, M.; Debije, M. G.; Florea, L.; Schenning, A. P. Temperature-Responsive 4D Liquid Crystal Microactuators Fabricated by Direct Laser Writing by Two-Photon Polymerization. *Small Struct.* **2022**, *3*, 2100158.
(28) Jampani, V. S. R.; Volpe, R. H.; Reguengo de Sousa, K.; Ferreira Machado, J.; Yakacki, C. M.; Lagerwall, J. P. F. Liquid crystal elastomer shell actuators with negative order parameter. *Sci. Adv.* **2019**, *5*, No. eaaw2476.
(29) Ditter, D.; Chen, W. L.; Best, A.; Zappe, H.; Koynov, K.; Ober, C. K.; Zentel, R. MEMS analogous micro-patterning of thermotropic nematic liquid crystalline elastomer films using a fluorinated photoresist and a hard mask process. *J. Mater. Chem. C* **2017**, *5*, 12635−12644.
(30) Traugutt, N. A.; Mistry, D.; Luo, C.; Yu, K.; Ge, Q.; Yakacki, C. M. Liquid-crystal-elastomer-based dissipative structures by digital light processing 3D printing. *Adv. Mater.* **2020**, *32*, 2000797.
(31) Mainik, P.; Hsu, L. Y.; Zimmer, C. W.; Fauser, D.; Steeb, H.; Blasco, E. DLP 4D Printing of Multi-Responsive Bilayered Structures. *Adv. Mater. Technol.* **2023**, *8*, 2300727.
(32) Zubritskaya, I.; Cichelero, R.; Faniayeu, I.; Martella, D.; Nocentini, S.; Rudquist, P.; Wiersma, D. S.; Brongersma, M. L. Dynamically Tunable Optical Cavities with Embedded Nematic Liquid Crystalline Networks. *Adv. Mater.* **2023**, *35*, 2209152.
(33) Zhang, Z. B.; Bolshakov, A.; Han, J. C.; Zhu, J. Q.; Yang, K. L. Electrospun core-sheath fibers with a uniformly aligned polymer network liquid crystal (PNLC). *ACS Appl. Mater. Interfaces* **2023**, *15* (11), 14800.
(34) Hisano, K.; Kurata, Y.; Aizawa, M.; Ishizu, M.; Sasaki, T.; Shishido, A. Alignment layer-free molecular ordering induced by masked photopolymerization with non-polarized light. *Appl. Phys. Express* **2016**, *9* (7), 072601.
(35) Feng, W.; Broer, D. J.; Grebikova, L.; Padberg, C.; Vancso, J. G.; Liu, D. Static and dynamic control of fingerprint landscapes of liquid crystal network coatings. *ACS Appl. Mater. Interfaces* **2020**, *12*, 5265−5273.
(36) Hisano, K.; Aizawa, M.; Ishizu, M.; Kurata, Y.; Nakano, W.; Akamatsu, N.; Barrett, C. J.; Shishido, A. Scanning wave photo-polymerization enables dye-free alignment patterning of liquid crystals. *Sci. Adv.* **2017**, *3*, No. e1701610.
(37) Wang, M.; Li, Y.; Yokoyama, H. Artificial web of disclination lines in nematic liquid crystals. *Nat. Commun.* **2017**, *8*, 388.
(38) Kim, D. S.; Čopar, S.; Tkalec, U.; Yoon, D. K. Mosaics of topological defects in micropatterned liquid crystal textures. *Sci. Adv.* **2018**, *4*, No. eaau8064.
(39) Ware, T. H.; McConney, M. E.; Wie, J. J.; Tondiglia, V. P.; White, T. J. Voxelated liquid crystal elastomers. *Science* **2015**, *347*, 982−984.
(40) Carlton, R. J.; Hunter, J. T.; Miller, D. S.; Abbasi, R.; Mushenheim, P. C.; Tan, L. N.; Abbott, N. L. Chemical and biological sensing using liquid crystals. *Liq. Cryst. Rev.* **2013**, *1* (1), 29−51.
(41) Chigrinov, V.; Kudreyko, A.; Guo, Q. Patterned photoalignment in thin films: physics and applications. *Crystals* **2021**, *11* (2), 84.
(42) Guo, Y.; Shahsavan, H.; Sitti, M. Microscale polarization color pixels from liquid crystal elastomers. *Adv. Opt. Mater.* **2020**, *8*, 1902098.
(43) Sørensen, B. E. A revised Michel-Lévy interference colour chart based on first-principles calculations. *Eur. J. Miner.* **2013**, *25* (1), 5−10.
(44) Zhang, Z.; Deng, C.; Fan, X.; Li, M.; Zhang, M.; Wang, X.; Chen, F.; Shi, S.; Zhou, Y.; Deng, L.; Gao, H. Three-Dimensional Directional Assembly of Liquid Crystal Molecules. *Adv. Mater.* **2024**, *36*, 2401533.
(45) Boothby, J. M.; Kim, H.; Ware, T. H. Shape changes in chemoresponsive liquid crystal elastomers. *Sens. Actuators, B* **2017**, *240*, 511−518.
(46) Harris, K. D.; Bastiaansen, C. W.; Broer, D. J. A Glassy Bending-Mode Polymeric Actuator Which Deforms in Response to Solvent Polarity. *Macromol. Rapid Commun.* **2006**, *27*, 1323−1329.
(47) Zhao, Y.; Xie, Z.; Gu, H.; Zhu, C.; Gu, Z. Bio-inspired variable structural color materials. *Chem. Soc. Rev.* **2012**, *41*, 3297−3317.
(48) Zhao, J.; Qiu, M.; Yu, X.; Yang, X.; Jin, W.; Lei, D.; Yu, Y. Defining deep-subwavelength-resolution, wide-color-Gamut, and large-viewing-angle flexible subtractive colors with an ultrathin asymmetric Fabry−Perot Lossy cavity. *Adv. Opt. Mater.* **2019**, *7* (23), 1900646.
(49) Kats, M. A.; Blanchard, R.; Genevet, P.; Capasso, F. Nanometre optical coatings based on strong interference effects in highly absorbing media. *Nat. Mater.* **2013**, *12*, 20−24.
(50) Liu, Z.; Luo, D.; Yang, K. L. Monitoring the two-dimensional concentration profile of toluene vapors by using polymer-stabilized nematic liquid crystals in microchannels. *Lab Chip* **2020**, *20*, 1687−1693.
(51) Zhan, X.; Luo, D.; Yang, K. L. Multifunctional sensors based on liquid crystals scaffolded in nematic polymer networks. *RSC Adv.* **2021**, *11*, 38694−38702.

https://doi.org/10.1021/acsami.4c20865
ACS Appl. Mater. Interfaces 2025, 17, 11100−11107